

E241 Final Report:

Sub-micron metal patterning on polymer substrates using nitride nanostencil

Anqi Ji and Skyler Selvin
E241 Spring 2021

Mentors:

Tony Ricco, Mark Zdeblick, Swaroop Kommera, and Graham J. Ewing

Table of Contents

1. Introduction	3
1.1 Motivation	3
1.2 Summary of work performed	4
1.3 Benefits to the SNF community.....	6
2. Fabrication and experiments.....	7
2.1 PDMS metal adhesion promotion.....	7
2.1.1 Metal polymer adhesion promotion using metal adhesion layer.....	7
2.1.2 Improving metal-polymer adhesion using a self-assembled monolayer - MPTMS	9
2.2 Nanostencil.....	11
2.2.1 Overview	11
2.2.2 LPCVD low-stress nitride deposition.....	12
2.2.3 Backside window patterning using Heidelberg.....	12
2.2.4 Reactive ion etching of backside nitride.....	12
2.2.5 KOH etching of Si wafer	13
2.2.6 JEOL patterning on SiNx membrane.....	14
2.2.7 Reactive ion etching of frontside nitride.....	15
2.2.8 Metal evaporation through nanostencil	16
3. Results and Discussions	18
3.1 PDMS metal adhesion results	18
3.1.1 Metal Adhesion layer	18
3.1.2 Self-assembled monolayer adhesion results	19
3.2 Nanostencil Results.....	21
Conclusions.....	29
Future Work	29
Acknowledgement.....	29
Budget.....	30
References.....	30

1. Introduction

1.1 Motivation

In recent years, increasing efforts have been dedicated to applying polymer materials to nano and micro devices. Different with dielectric materials, polymers exhibit a wide range tunable property. For example, the optical property and the shape of many polymers (PDMS, PEDOT, liquid crystal elastomer, etc.) can be mechanically or thermally tuned. Such property is extremely beneficial to the plasmonics community where actively tunable devices are in great demands. Fig.1.1 shows the typical layout of a plasmonic device, in which a dielectric layer is sandwiched between metal gratings and a continuous metal film. The optical properties (reflection, absorption, diffraction) of a plasmonic device are highly sensitive to the gap material and size. As a result, a simple replacement of dielectric layer to a polymer film would transform a passive device into an active device that can be used in beam steering and biomedical sensing.

However, the fabrication of polymer based plasmonic devices faces two main challenges. First, the adhesion between metals and polymers are rarely explored. For each type of polymer and metal combination, a customized adhesion method needs to be established. Second, many polymers are not compatible with standard resist-based lithography techniques. Applying resists or solvents to polymers can lead to swelling (PDMS) and dissolving (liquid crystal elastomer) of the polymer films. The chemical incompatibility with resists greatly limits its integration into plasmonic devices.

Limited by the time and budget for this class, we limit ourselves to PDMS, a deformable polymer, as the polymer material of interest. In the first part of the project, we explore and compare various methods that can potentially promote the PDMS-metal (Au/Al) adhesion. In the second part of the project, we establish a process flow of resist-free nanostencil lithography technique that allows sub-micron metal patterning on a polymer substrate.



Fig. 1 Schematic layout of a plasmonic device.

From top to bottom: metal gratings, dielectric film/polymer, metal film

1.2 Summary of work performed

Metal-polymer adhesion promotion

In this class, we explore two methods to improve adhesion between PDMS and metal. The first method is through metal adhesion layer and the second is through surface modification. In Fig. 2, we show the process flow of the second method. A self-assembled monolayer named MPTMS functionalizes the surface with thiol group. The thiol group is proved to be very adhesive to gold. Our work establishes a step-by-step SOP on how to functionalize a surface with MPTMS.

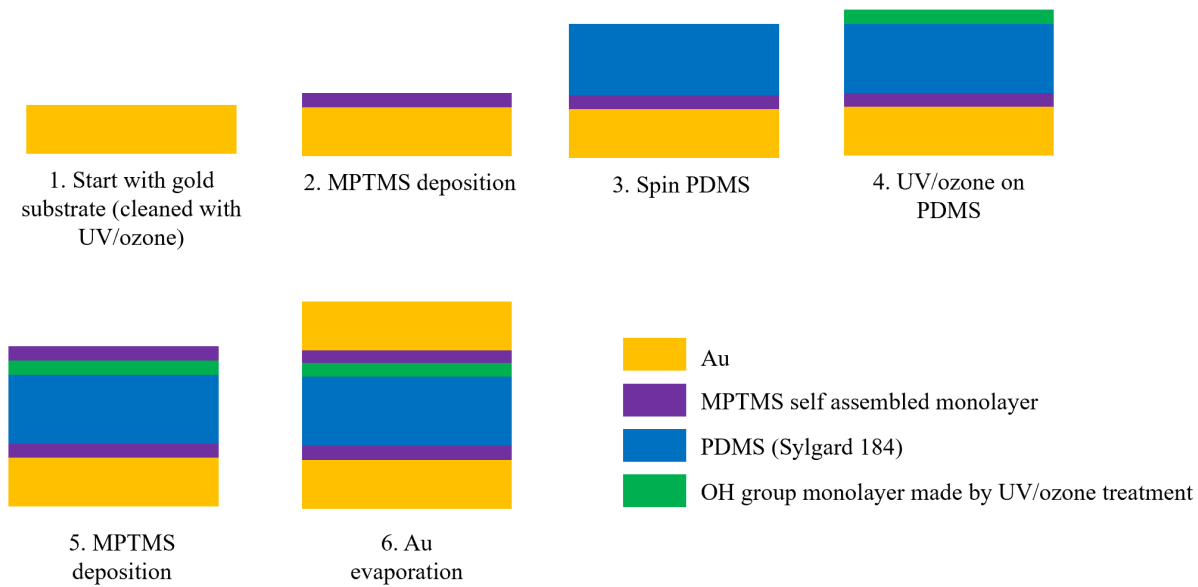


Fig. 2. Process flow of adhesion promotion through surface functionalization (MPTMS)

Nanostencil lithography

In Fig. 3, we show the workflow of our study on nanostencil lithography. We first fabricated a nitride nanostencil with sub-micron patterns. Then, we evaporate metal through a nanostencil onto our target wafer. We used optical images to confirm the sturdiness of the nitride membranes with different patterns. At the same time, we used AFM and SEM to study the evaporated metal patterns on the target wafer.

Our work aims to answer 3 key questions:

- What is the relationship between grating geometry and mechanical stability?
- How vertical are the sidewalls of evaporated metal patterns on target wafer?
- How does the metal evaporation rate change as the aperture size on nanostencil shrinks?

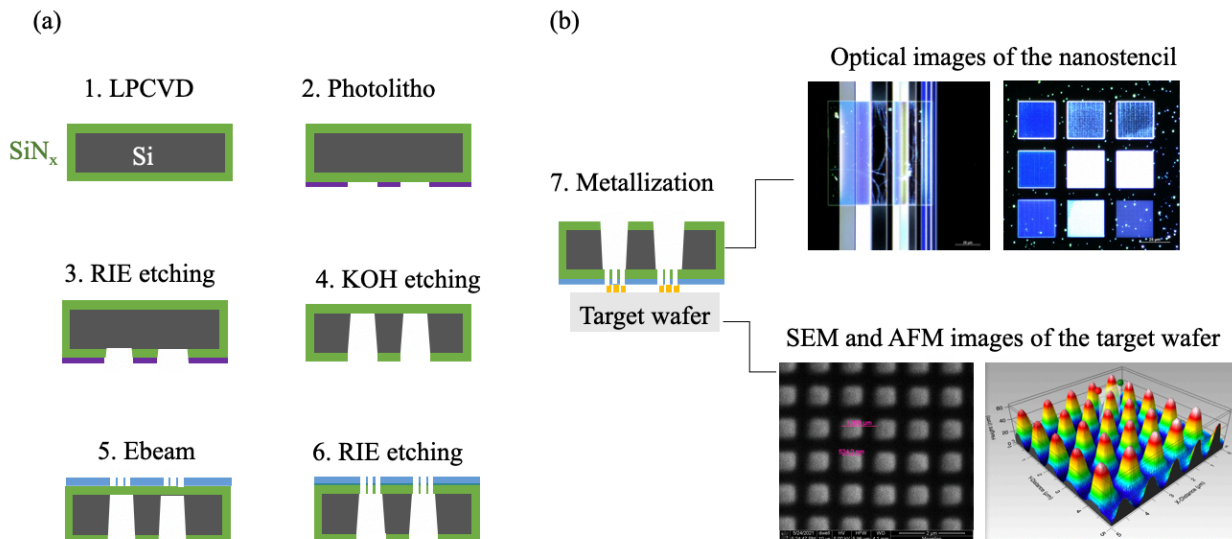


Fig. 3. The overview of workflow for nanostencil lithography. a, The fabrication of a nitride nanostencil. **b,** The evaluation of nitride nanostencil through optical microscopy, SEM and AFM.

1.3 Benefits to the SNF community

Our work uniquely benefits SNF mostly in two aspects. First, our work on metal-polymer adhesion promotion offers a deep understanding of the surface chemical properties of polymers. It offers a guideline to those who are interested in interfacing metal with a polymer. Second, the process flow we established for nanostencil lithography technique provides a highly flexible and universal way to pattern sub-micron features on an arbitrary wafer. Because the method only involves a single step evaporation on the final wafer, it can be applied to any wafer that is chemical and heat sensitive.

As we progress on our project, we also develop several standard operating procedures (SOP) that haven't been previously reported at SNF and SNSF. Below are some highlighted processes we explain in the SOP.

1. PDMS-Au adhesion promotion using self-assembled monolayer (MPTMS).
2. Vacuum free resist spin coating.
3. Frontside to backside alignment for Ebeam lithography (JEOL).
4. Collimated metal evaporation using AJA

2. Fabrication and experiments

2.1 PDMS metal adhesion promotion

Metals have a wide range of adhesion characteristics. For example, aluminum naturally has strong adhesion to PDMS while noble metals such as Au barely sticks to polymer substrates. In this project, we attempted two methods to promote PDMS adhesion to gold (Au).

The first method is to use titanium (Ti) adhesion layer between gold and PDMS. The Ti layer forms strong chemical bonds to the PDMS and the Au, thus sticking the two materials together. However, Ti is known to diffuse into grain boundaries of Au and can interfere with the chemical and optical properties of Au. To prevent this, we used a palladium diffusion boundary between the Ti layer and the gold layer. Other metals such as chromium can also be used as an adhesion layer.

The second method is through a self-assembled monolayer (SAM) to functionalize the surface. MPTMS is a polymer that introduce thiol group (-SH) to a surface. The thiol group was proved to strongly adhere to Au. Because the SAM is less than 1 nm, this method particularly suits for photonic and plasmonic devices that are very sensitive to index contrast at interfaces.

We used sticky tape to test the adhesion of metals. The test is performed in the following way. A Scotch magic tape was applied the top surface of a sample. Then, we pressed the tape with a Q tip. Then we peeled off the tape and examine how much metal remains. Although other methods may yield more quantitative result), our method is the easiest for a qualitative assessment.

2.1.1 Metal polymer adhesion promotion using metal adhesion layer

To test the adhesion of an evaporated metal to a PDMS substrate, we created a design of experiments, shown in Table. 1. The top three experiments tested the adhesion of aluminum to PDMS. We experimented with directly depositing the aluminum without an adhesion layer (test 1), as well as treating the PDMS with UV/O₃ and MPTMS (tests 2 and 3). Please see the next section for more information on MPTMS.

The bottom three experiments tested the efficacy of using a Ti adhesion layer on PDMS. In sample 4, we deposited the Ti without the gold. In sample 5, we deposited Ti then gold without breaking the vacuum. In sample 6, we deposited Ti then broke the vacuum to allow of TiO₂ to form on the Ti surface.

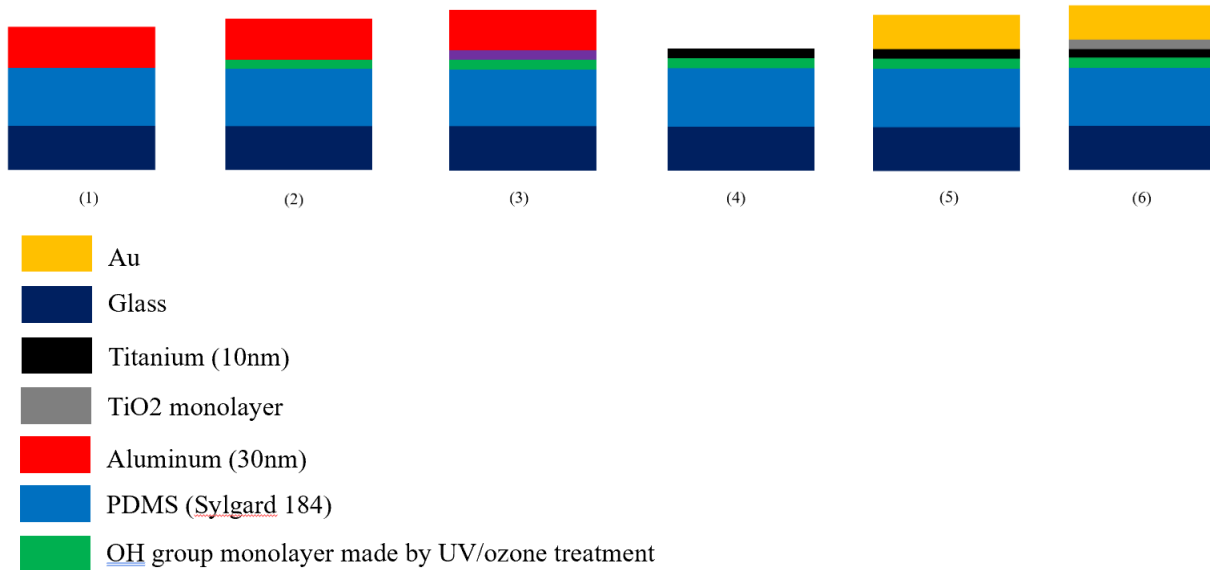


Fig. 4 Experiments testing metal-PDMS adhesion promotion.

Table 1. Design of experiments for metal adhesion layer preparation

Test no	Adhesion test	Substrate	Bottom adhesion	Middle layer	Top adhesion	Top layer
1	Top	Glass	UV/O ₃	PDMS	-	Al
2	Top	Glass	UV/O ₃	PDMS	UV/O ₃	Al
3	Top	Glass	UV/O ₃	PDMS	UV/O ₃ + MPTMS	Al
4	Top	Glass	UV/O ₃	PDMS	UV/O ₃	Ti
5	Top	Glass	UV/O ₃	PDMS	UV/O ₃ +Ti	Au
6	Top	Glass	UV/O ₃	PDMS	UV/O ₃ +Ti+TiO ₂	Au

Metal deposition methods

In this study we use electron beam evaporation (*aja_evap*) to deposit the metals of interest. It has the advantage of directional deposition compared to sputtering.

Al deposition:

30 nm aluminum at a rate of 1 A/s.

Ti deposition:

10 nm titanium at a rate of 0.5 A/s.

Au deposition:

Immediately after Ti deposition and without breaking vacuum (except in the case of sample 6), 30 nm gold as deposited at a rate of 0.5 A/s.

PDMS deposition

We used ~25 um thick spun PDMS layer for our experiments. This thickness was visible to the naked eye when peeled off during adhesion tests and is near the minimum thickness possible without dilution of PDMS in a solvent. This process was carried out in the Allen 155 lab (Mavericks). See SOP for details.

UV/O₃ plasma treatment

This process was carried out in the Brongersma chemical lab with a UV/O₃ machine (Jelight model 24).

1. UV/O₃ 5 min on PDMS.
2. Surface was exposed to air for a few min after UV/O₃.

2.1.2 Improving metal-polymer adhesion using a self-assembled monolayer - MPTMS

MPTMS a molecule that has a thiol (-SH) group on one end, shown in Fig. 5. The thiol group is known to adhere well to gold ¹⁻³. The trimethylsilyl groups on the other end adhere well to uncured PDMS. Thus, this molecule functionalizes a gold surface to adhere well to PDMS. However, MPTMS does not adhere well to a cured PDMS surface. Thus, for the top layer adhesion and to adhere a cured PDMS layer to evaporated gold, we must first functionalize the PDMS by treating the PDMS with oxygen plasma and exposing to air for ~10 min. The UV/O₃ creates hydroxyl groups on the surface of the PDMS and will bond well with the trimethylsilyl groups on the MPTMS.

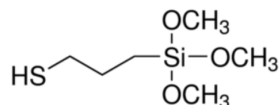


Fig. 5 Diagram of MPTMS

Design of experiments

Table 2. Design of experiments for metal-polymer adhesion through MPTMS

Test no	Adhesion test	Substrate	Bottom adhesion	Middle layer	Top adhesion	Top layer
1	Bottom	Au	-	PDMS	-	Au
2	Bottom/top	Au	-	PDMS	-	-
3	Bottom	Au	MPTMS	PDMS	-	Au
4	Bottom/top	Au	MPTMS	PDMS	-	-
5	Bottom	Au	MPTMS	PDMS	MPTMS	Au
6	Bottom/top	Au	MPTMS	PDMS	MPTMS	-
7	Bottom/top	Au	-	PDMS	MPTMS	Au
8	Top	Glass	UV/O ₃	PDMS	-	Au
9	Top	Glass	UV/O ₃	PDMS	UV/O ₃	Au
10	Top	Glass	UV/O ₃	PDMS	MPTMS	Au
11	Top	Glass	UV/O ₃	PDMS	UV/O ₃ + MPTMS	Au
12	Top	Glass	UV/O ₃	PDMS	UV/O ₃ & air + MPTMS(2)	Au

To optimize the process to use MPTMS for surface modification, we design the experiment in the following way, shown in Table. 2. By using a gold substrate, PDMS middle layer, and evaporated gold on top, we can test the relative adhesion of the top and bottom layers. These tests are shown by the “bottom + top” adhesion test in the table. Two different processes for the MPTMS deposition were used. The first did not use toluene to remove unreacted oligomers after SAM deposition, while the second used a 90 min soak in anhydrous toluene.

Methods to deposit MPTMS

There are three common ways to deposit MPTMS:

1. Liquid deposition: soak a sample in a solvent in which MPTMS is dissolved.
2. Spin coating: spin coat a sample in a solvent in which MPTMS is dissolved.
3. Vapor deposition: place MPTMS vial and sample in a vacuum chamber and allow MPTMS to evaporate and coat the sample.

All three methods are known to give good results. However, the liquid deposition method has been shown to be superior for functionalizing gold to adhere to PDMS. Moreover, it is the simplest method and does not contaminate a vacuum chamber with MPTMS.

MPTMS on Au:

1. 60 uL of (3-Mercaptopropyl) trimethoxysilane 95% from Sigma Aldrich was dissolved in 40 ml of anhydrous ethanol to make 8 mM solution.
2. Au substrates were cleaned with acetone-> methanol -> IPA spray washes.
3. Au substrates were soaked in MPTMS solution for 40 min.
4. Spray wash with ethanol and N₂ gun dry.

MPTMS on PDMS:

1. 60 uL of (3-Mercaptopropyl) trimethoxysilane 95% from Sigma Aldrich was dissolved in 40 ml of ethanol to make 8 mM solution.
2. Substrate with cured PDMS was soaked for 22 min in MPTMS solution.
3. Spray washed with ethanol then dried with N₂ gun.

Toluene dissolution of unreacted oligomers

Toluene can be used to remove unreacted oligomers from both the PDMS and MPTMS. By soaking the SAM coated PDMS in toluene for a few hours, unreacted MPTMS and uncured PDMS are eliminated.

MPTMS (2) on PDMS:

1. 60 uL of MPTMS was dissolved in 40 ml of ethanol to make 8 mM solution
2. PDMS substrates were soaked in MPTMS solution for 2 hours
3. Spray wash with ethanol then dry with N₂ gun
4. Toluene soak for 1.5 hours
5. Ethanol spray wash
6. Blow dry and then air dry for 0.5 hours

2.2 Nanostencil

2.2.1 Overview

Nanostencil lithography is a shadow mask based patterning technique. High resolution features can be defined on the shadow mask using traditional lithography methods such as photolithography or electron beam lithography. A final step of deposition, etching or ion implantation through the membranes allows the inverse pattern of the membrane to be transferred onto the target substrate⁴.

Different from traditional methods, nanostencil lithography does not involve any resist/solvent or heating of the target substrate. This truly unlocks the possibility to pattern on top of unconventional substrates that are vulnerable to various chemical and physical processes. Besides dielectric substrates, previous studies showed that nanostencil lithography can be used to pattern on top of substrates that are made of semiconductors⁵, organics⁶, 2D materials⁷, and magnetic materials^{8,9}. Furthermore, by variation of the final step, the patterned materials can be metals, dielectrics, crystals, 2D materials or even cells and proteins^{10,11}.

The smallest feature size demonstrated using nanostencil lithography is comparable to that of Ebeam lithography. Gold nanorods with 20-50 nm diameter and 100 nm pitch were demonstrated¹². The same paper showed the width of the lines in the nanostencil membrane could be as thin as 50 nm. The precise control of nanostencil geometries allows small features with various filling factors to be patterned using this method.

Despite the extensive studies on nanostencil lithography, this technique faces two main challenges. The first challenge relates to the mechanical stability of the nanostencil. As the pattern size shrinks, the patterns on the membrane would eventually become fragile and thus limiting the possible geometry on the possible patterns. Furthermore, the resolution of the final structures can be affected by the intrinsic gap between the nanostencil and the target substrate^{10,13}. With a common gap size from 2-30 um, the final patterns can be blurred with gradual side walls.

Our project attempts to study 1) the influence of geometries on the mechanical stability of the nanostencil, and 2) the sidewall slope influenced by the gap and evaporation condition. Our work builds on the previous studies on nanostencil with modification of certain steps to achieve to our goals. Fig. 6 shows our process flow. First, we deposited low stress silicon nitride on a silicon wafer using low pressure chemical vapor deposition (LPCVD). Then we used photolithography followed by a RIE etching to form windows on the backside. After KOH etching, nitride membranes are formed on the frontside of the wafer. Then we used Ebeam lithography to form sub-micron level patterns directly on the membrane. After RIE etching, a patterned membrane was defined on the front side. Finally, we directly contacted the membranes and a target wafer for the metallization. To evaluate the performance of the nanostencil, we captured images of both the membranes and the target wafer.

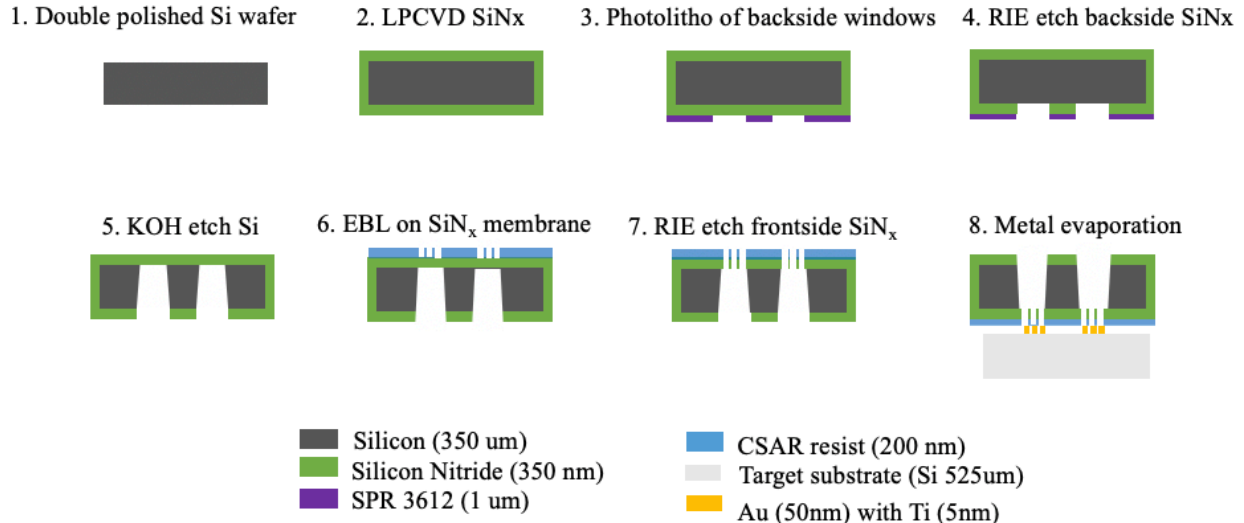


Fig. 6 Fabrication process of silicon nitride nanostencil

2.2.2 LPCVD low-stress nitride deposition

Prior to the LPCVD silicon nitride deposition, the doubled polished silicon went through a standard RCA cleaning procedure. To achieve best mechanical stability of the membranes, a low stress nitride recipe (LSN3 on thermoconitride) was adopted. Silicon nitride was deposited at a moderately high temperature (850 °C) and at a low pressure of 250 mTorr. The gas flow is composed of 300 sccm dichlorosilane (SiCl₂H₂) and 28 sccm ammonia (NH₃). The silicon nitride produced by this recipe has refractive index around 2.2 and stress less than 100 MPa. The deposition rate is approximately 7 nm/min. With a 48 min deposition time, 350 nm Si₃N₄ films were formed on both sides of the silicon wafer.

2.2.3 Backside window patterning using Heidelberg

The backside window of the nanostencil was defined using Heidelberg. The resist we used is a positive tone resist, SPR3612 of 1 μ m thick. The windows are in square shape of three sizes: 600 μ m, 800 μ m and 1000 μ m. The pattern is exposed with dose 70 and defocus of -2.

2.2.4 Reactive ion etching of backside nitride

The exposed silicon nitride on the backside of the wafer is etched away using reactive ion etching (RIE). In Table. 3, we list the details of the nitride etching recipe we used. Prior to processing the real wafer, we tested the etching rate of silicon nitride using a test wafer that has the same thickness of nitride as the real wafer. An etching time of 5 min is sufficient to fully remove a 350 nm nitride film, shown in Fig.7. Note that our goal is only to fully etch away the exposed silicon nitride, a 10% over-etch is adopted on the real wafer to guarantee that there no nitride is left. Our 1 μ m SPR3612 mask is etched 230 nm during the nitride etching.

Table 3. Nitride dry etching recipe (SNF Oxford RIE)

Recipe name	OA-SiN-RIE1
Gas flow	75: 15: 10 = CHF ₃ : CF ₄ : O ₂
Forward power	200 W
DC bias	508 V

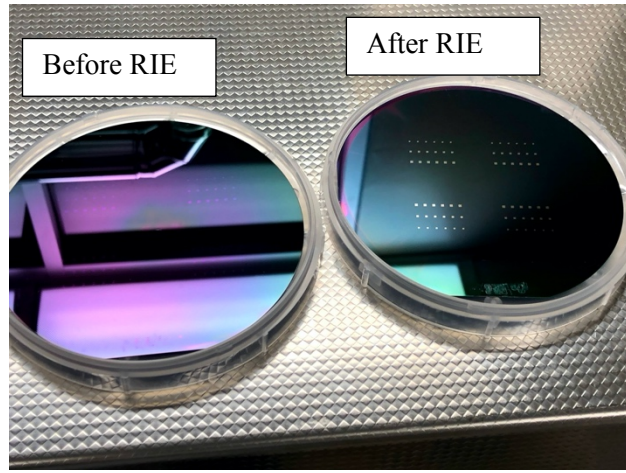


Fig. 7 Silicon wafers before and after RIE etching.

2.2.5 KOH etching of Si wafer

To create a nitride membrane, the entire Silicon wafer needs to be etched through to leave nothing but a silicon nitride film on one side. We use potassium hydroxide (KOH) to etch silicon because of the extremely high selectivity between Si and nitride. The KOH etch rate of $\langle 100 \rangle$ Si depends on the temperature and the concentration of KOH. At 80°C with 30% KOH we expect an etch rate of about 75 $\mu\text{m}/\text{h}$. The etching happens at particular crystal plane, resulting in a 54.7° angle in the Si wafer, as shown in Fig. 8(c).

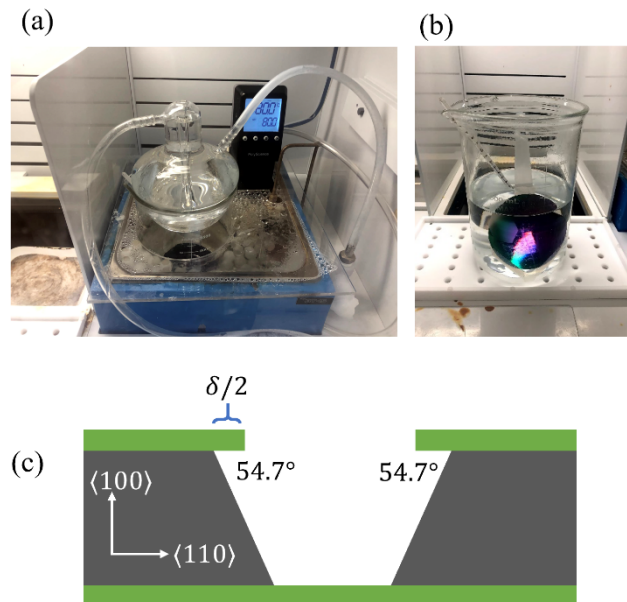


Fig. 8 Setup of KOH etching. a, b, setup of KOH etching. c, KOH etching SiN_x membrane diagram.

2.2.6 JEOL patterning on SiN_x membrane

Pattern design of the gratings

In Fig. 9, we show the designed grating patterns for the nitride membrane. To fully investigate how geometry influences the stability of the nanostencil, we vary the grating length, period, filling factor as well as the shape of the grating (1D versus 2D). To eliminate the influence from other factors (nitride stress, handling of the wafer, dry etching process), all patterns are defined on the same wafer. Thus, they experience the same prior and following processes.

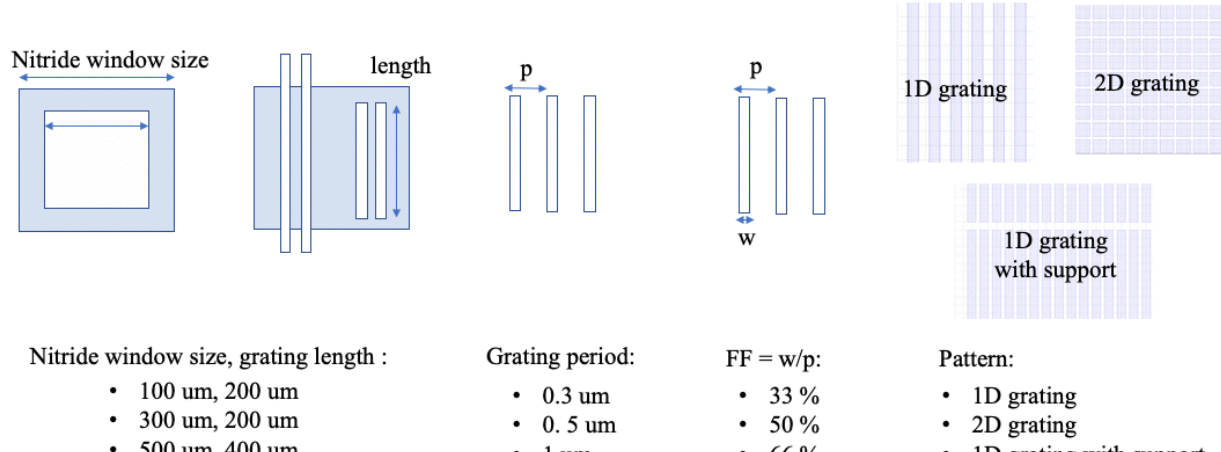


Fig. 9 Pattern design of the nanostencil. Various geometries are patterned on the same wafer to yield a fair comparison of their mechanical stability.

Vacuum free Ebeam resist spin coating

Note that our wafer now has nitride silicon membranes, we have to spin coat ebeam resist without vacuum from the back. This can be achieved by attaching the nanostencil wafer on top of a 6-inch carrier wafer using tapes and bumpers, shown in Fig. 10. The 6-inch wafer was directly placed on top of a spinning chuck in a standard fashion. The tapes and the bumpers forbid the wafer from leaving the carrier wafer during spinning. In principle, only 4 small tapes can fix the wafer the 6-inch wafer, see Fig. 10 (b). However, we found that Ebeam resist could leak to the back of the nanostencil wafer and make it hard to separate the two wafers after spin coating. Therefore, we recommend using tapes around the wafer (Fig. 10(a)) to prevent such leaking. A detailed SOP of the spin coating process is reported in a separate document.

After preparing the wafer, we spin coated roughly 200 nm (3000 rpm 60 seconds) of CSAR 9% on the wafer. The resist is baked at 180°C for 1min.

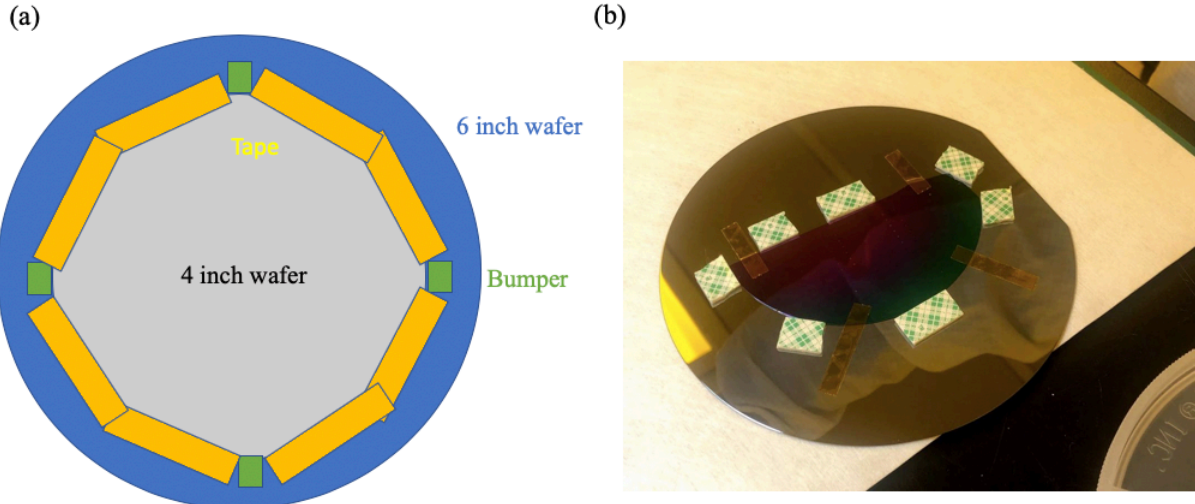


Fig. 10 Vacuum free spin coating preparation. **a**, Schematic of the wafer attachment to a carrier wafer. **b**, photo of our implementation.

Exposure on Ebeam (JEOL)

The exposed patterns need to be aligned to the nitride window location. The alignment was done in two steps, 1) a rough alignment using an optical microscope. 2) a precise alignment using SEM on JEOL. A detailed SOP for this alignment is included in our SOP. With a careful alignment, the alignment error should be less than 10 um.

After the alignment, the pattern is exposed at the EOS3 2nA 60um mode. Half of the wafer was exposed at dose 400 and the other half at dose 500. Later, the resist was developed in xylens for 40 seconds followed by multiple rinses in isopropanol.

2.2.7 Reactive ion etching of frontside nitride

Choice of plasma etcher

The frontside nitride etching was performed using Oxford RIE at SNSF. Because the frontside nitride has to be etched through, the ion beam will eventually pass through the membrane and arrive at the backside of the wafer. Therefore, we need to make sure the back holder of the wafer cannot be damaged by the ions. The Oxford RIE at SNF has a backside helium cooling system beneath the wafer which can be damaged by the ions. As a result, we choose to use the etcher at SNSF, which does not have back helium cooling.

Confirmation of etching through

The details of the etching recipe are listed in the Table. 4. As we know, the etching rate depends on the mask geometry. The smaller the pattern opening, the slower the etch rate. To ensure the nitride membrane is fully etched through for all patterns, we adopted an etch time (10 min) that is 25% longer than what is needed for a unpattern nitride film with the same thickness (8 min). This is allowed because the etching mask (Csar 200 nm) and nitride has high etching selectivity (> 3:1) with this recipe. The Csar mask would still remain despite of the slight over-etch of the

nitride. As later confirmed, for the grating width between 100 nm – 900 nm, 25% over-etch was confirmed to be sufficient to etch through the patterned membranes.

Table 4. Nitride dry etching recipe (SNSF Oxford RIE)

Recipe name	Frank slow nit
Gas flow	15: 45: 30 = CHF ₃ : CF ₄ : Ar
Forward power	200 W
DC bias	440 V
Pressure	100 mTorr

The simplest way to confirm the etching through is by optical microscopy. We show the optical images of the wafer before and after RIE etching in Fig. 11. Before the etching, the nitride membrane appeared to be a bright-colored and uniform film. By contrast, after the RIE etching, some areas appeared to be completely dark, which indicates zero reflection from the surface. Such areas can be confidently claimed as fully etched. In a dark field configuration, we can visualize the extremely thin broken SiN_x beams hanging in the dark air region. This method is fundamentally limited by the resolution of the microscope. Extremely small gaps (< 300 nm) can be difficult to resolve. However, it is an easy and quick method for an estimate.

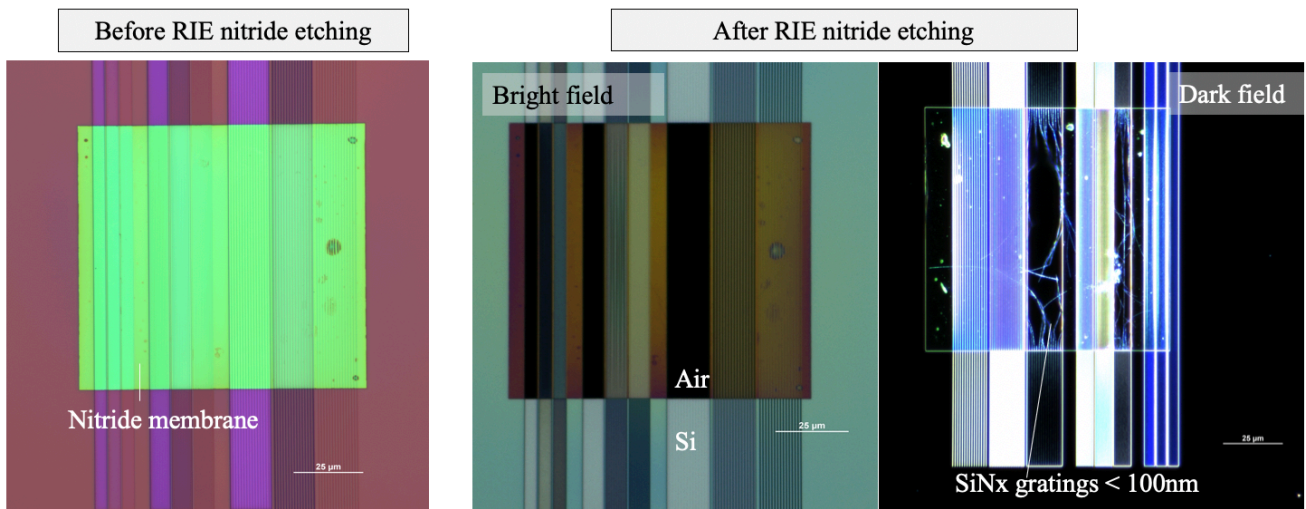


Fig. 11 Optical microscope images of the nanostencil before and after RIE etching. The optical microscope is operated in the reflection mode. The scale bars correspond to 25 μm length. (Left: before, bright field; Middle: after, bright field; Right: after, dark field)

2.2.8 Metal evaporation through nanostencil

Choice of metal evaporator

In nanostencil lithography, metals are evaporated through a physical hard mask clamped on the target wafer. Different with the metal evaporation in a standard lift-off process, there is an intrinsic gap (2-30 μm) between the mask and the target wafer. As a result, unavoidable shadowing and diffusion appear on the evaporated structures as shown in Fig. 12.

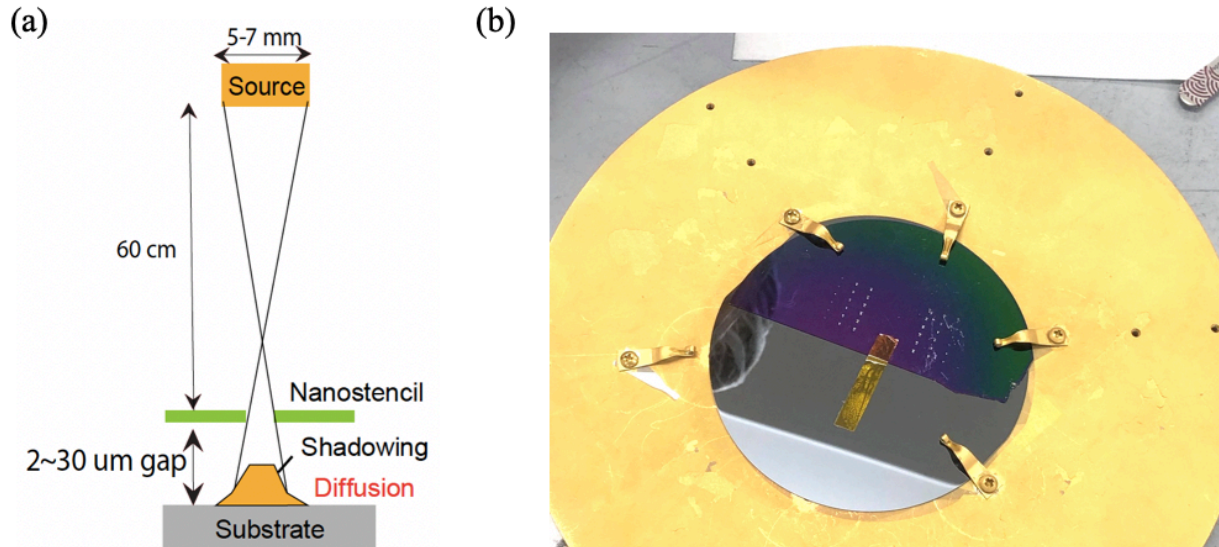


Fig. 12 Intrinsic gap between clamped wafers during metal evaporation (a) Illustration of the origin of shadow and diffusion. The dimensions and distance indicated here represent a common setup of AJA evap. (b) Clamping method used in this project.

To minimize the level of shadow, a metal evaporator with the following properties is preferred:

1. Highly directional metal particles. From this perspective, an ebeam evaporator is always preferred over a sputtering system.
2. Long distance between the metal source and the substrate. This ensures a small divergence angle through the stencil.
3. Small source crucible size. A point source can further eliminate the divergence angle arriving on the substrate.

The metal evaporator we chose is an ebeam evaporator (AJA evap). The distance between the source and the substrate is 24 inches. The diameter of the metal crucible is roughly 2 cm. The maximum volume inside the crucible is 150 cc.

Metal deposition

Condition 1:

- A 5 nm thick titanium film was first deposited on (0.1 A/s) the Si wafer as an adhesion layer. Afterwards, 50 nm thick gold was evaporated at a speed of 2 A/s.
- The Ebeam scanning size on Au and Ti source is roughly 5-7 mm.
- The substrate rotation performed at a low speed.

Condition 2:

- A 5 nm thick titanium film was first deposited on (0.1 A/s) the Si wafer as an adhesion layer. Afterwards, 50 nm thick gold was evaporated at a speed of 0.5 A/s.
- The Ebeam scanning size on Au and Ti source is reduced to ~1mm diameter (the smallest on the tool, this cannot be directly measured).
- The substrate rotation is disabled.

3. Results and Discussions

3.1 PDMS metal adhesion results

3.1.1 Metal Adhesion layer

The results for the Al-PDMS tests are shown in the Fig. 13. Without any special treatment, Al shows good adhesion to PDMS. UV/O₃ treated PDMS shows similar adhesion, while PDMS modified by MPTMS has poor adhesion to aluminum.

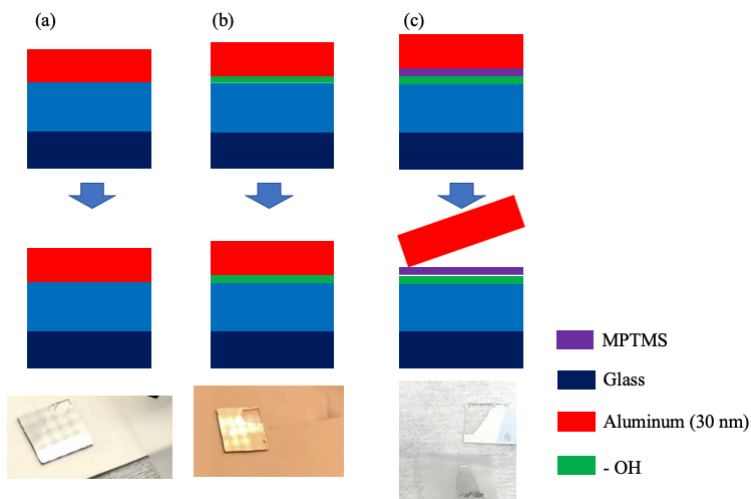


Fig. 13. Al-PDMS adhesion promotion through metal adhesion layer. Top row: sample construction; Middle row: after the tape adhesion test; Bottom row shows: photo after peeling.

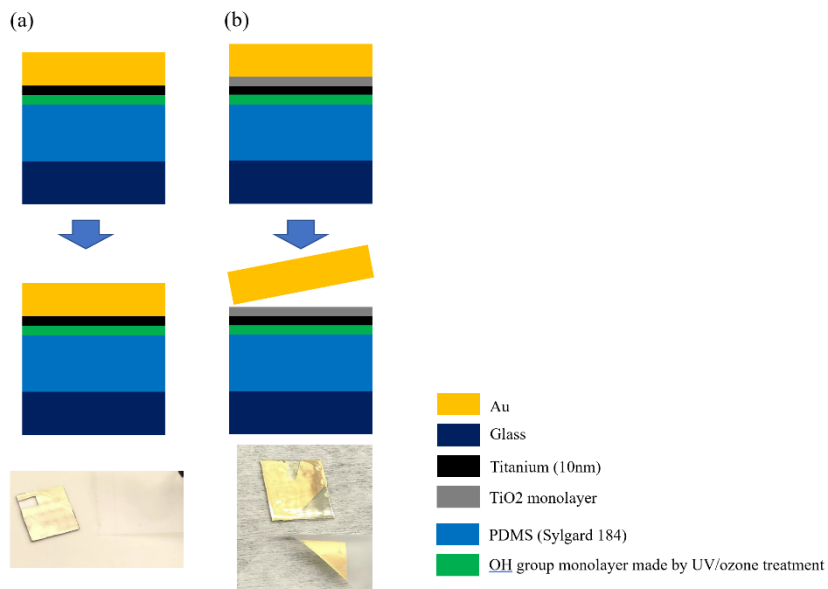


Fig. 14. Au-PDMS adhesion promotion through metal adhesion layer. Top row: sample construction; Middle row: after the tape adhesion test; Bottom row shows: photo after peeling.

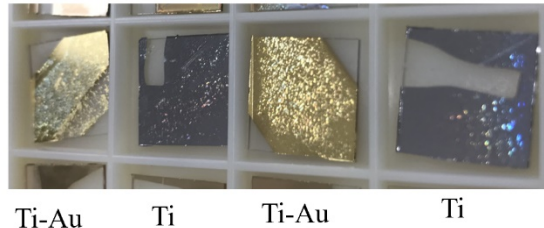


Fig. 15 Cracks appear when titanium was deposited on PDMS. We see two repetitions of each sample. The two golden colored chips are sample (5) above and the two Ti colored samples are sample 4.

The results for the PDMS-Au adhesion tests are shown in the Fig. 14. The adhesion is strong when there is no vacuum break between Ti and Au deposition. Therefore, Ti acts as an effective adhesion layer when it is not oxidized. However, we notice significant cracks in the gold on the same sample. When we evaporated only Ti on the UV/O₃ treated PDMS substrate and also observed these cracks, as shown in Fig. 15. The evaporator is at a higher voltage when depositing Ti than other metals. Thus, we suspect the cracks might originate from difference in the thermal expansion coefficient between the PDMS and Ti materials. This reduces the usability of Ti as an adhesion layer on PDMS and similar substrates.

3.1.2 Self-assembled monolayer adhesion results

Bottom Au - Top PDMS adhesion

Without any adhesion layer, the native adhesion between a gold substrate and spun PDMS was quite weak. Immediately after PDMS deposition, we observed visible signs of the polymer pulling away from the gold substrate. By comparing sample 1, 2 and 3,4, we discovered that MPTMS is very effective in improving the bottom layer adhesion, as shown in Fig. 16. None of the scotch tape tests were able to remove the PDMS from gold when MPTMS is in between. Furthermore, the PDMS remained on the substrate during all the tape tests.

Bottom PDMS - Top Au adhesion results

The first attempts to enhance adhesion were on samples 5, 6, and 7 where only MPTMS was deposited without UV/O₃ treating the PDMS layer. This however showed no noticeable improvement in the adhesion of gold.

We then experimented with the effects of UV/O₃ treating the PDMS before SAM deposition in samples 9, 11, and 12. We found that UV/O₃ treatment or MPTMS alone does not enhance adhesion of evaporated gold to cured PDMS. However, the combination of UV/O₃ treating the PDMS substrate and then depositing MPTMS gave a noticeable improvement in the adhesion of gold to PDMS (samples 11 and 12).

For the two different types of UV/O₃ treatment attempted as well as two types of MPTMS deposition, there was no significant difference between the results. However, it appears that sample 11 had slightly better results. Thus, the optimal way to prepare the sample is the way adopted in sample 11: UV/O₃ treatment with only a few minutes of wait time before immersion into MPTMS solution and no toluene treatment of the cured PDMS & MPTMS stack.

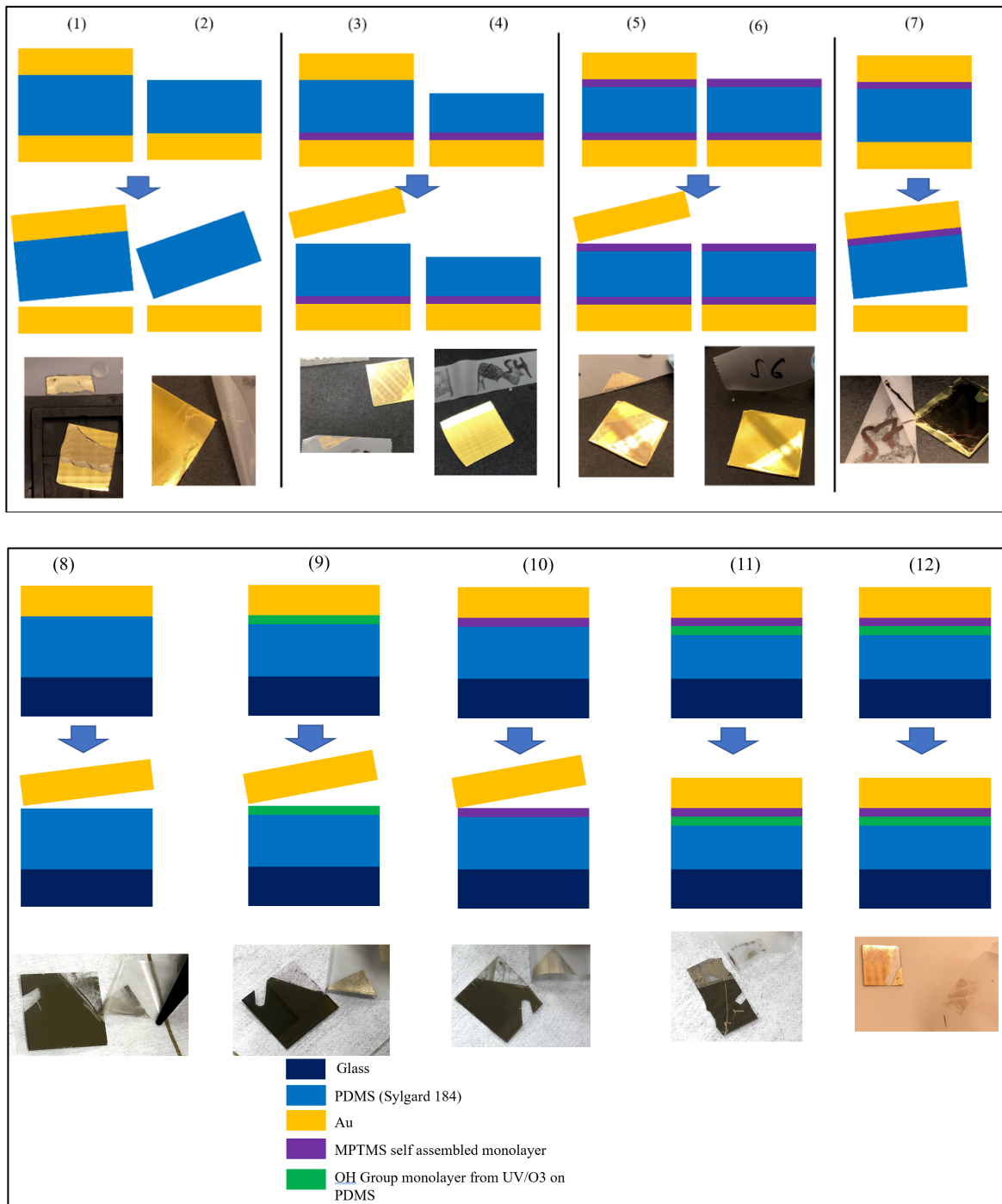


Fig. 16. Au-PDMS adhesion promotion through MPTMS. Top row: sample construction; Middle row: after the tape adhesion test; Bottom row: photo after peeling.

3.2 Nanostencil Results

3.2.1 Mechanical stability of the nitride membranes

Influence from grating type

We first compare the optical images of nanostencil with various grating geometry in Fig. 17. When the gratings are 1D, most beams are stably suspended except for the ones that are 100 nm thin, shown in Fig. 17(a). It matches our expectation that thicker gratings are sturdier. At the same time, the grating period does not strongly affect the mechanical stability. The 100 nm thin gratings with both 1000 nm period and 500 nm are broken. In Fig. 17(b), we show gratings of 300 period and 100 nm width. We vary the density and size of the mechanical supports. The gratings are all broken. This indicates that sparse horizontal supports do not improve the mechanical stability of the thin gratings very much. However, when the gratings are fully crossed in 2D as shown in the Fig. 17(c), the mechanical stability is significantly improved. All gratings as small as 100 nm fully survive the fabrication process. To sum up, grating type strongly influences the mechanical stability of the nanostencil. The 2D cross gratings are significantly sturdier than the 1D gratings.

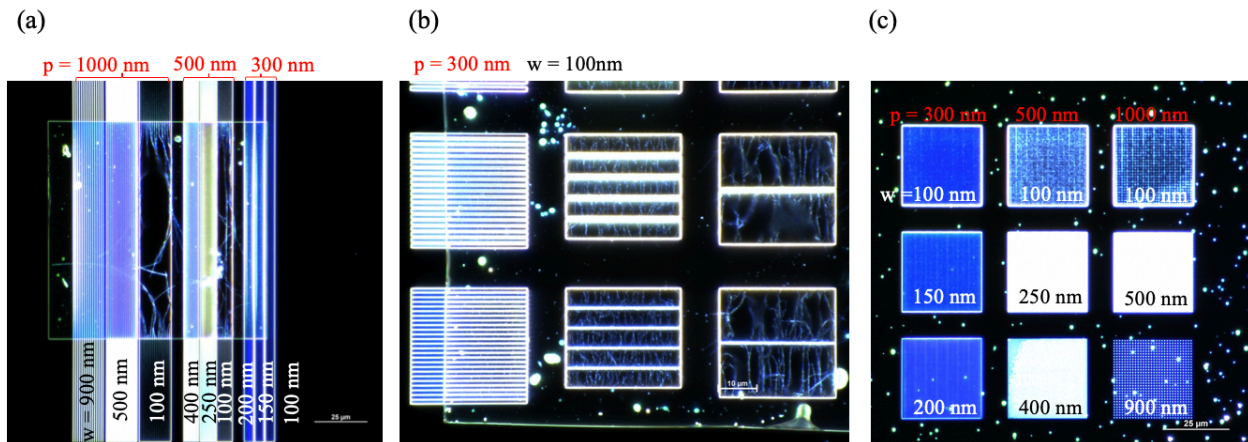


Fig. 17 Optical images of the nanostencil of various grating geometry. a, 1D gratings of different size and filling factor. b, 1D gratings with horizontal supports. c, 2D gratings. The red colored numbers indicate the grating periodicity. The black and white numbers indicate the grating width of the nanostencil (the size of the beams instead of the opening).

Influence of grating length on the bowing of the gratings

In Fig. 18, we show the images of gratings of different lengths. The top row shows the optical images of the nanostencil, while the bottom row shows the SEM images of the corresponding evaporated pattern. The only difference of the (b) and (c) nanostencil is the length of the suspended gratings. The 100 μm long gratings are fully parallel, while the 200 μm long ones start to attract and repel each other after a certain distance ($\sim 20 \mu\text{m}$) from the end of the grating. This shows that reducing the grating length lead to less bowing.

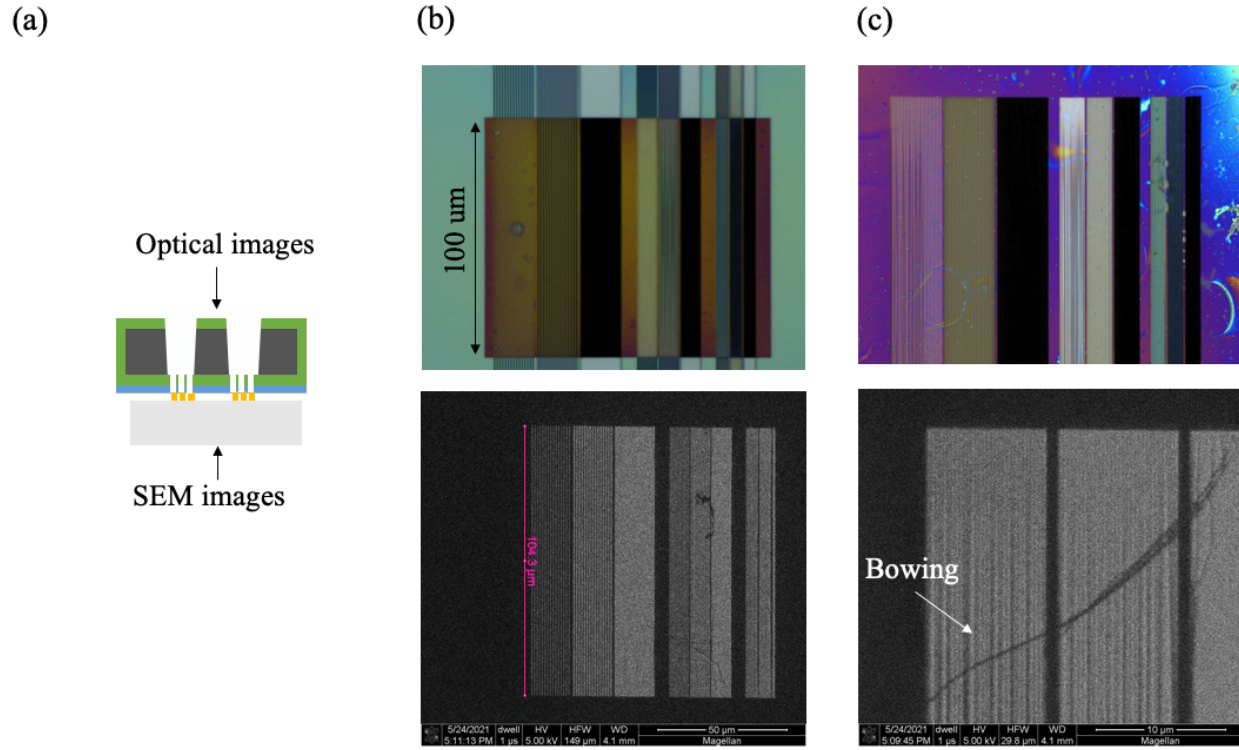


Fig. 18 Bowing of the gratings with different length. **a**, Schematic of how images were captured. **b**, 100 μm long gratings. **c**, 200 μm long gratings.

Resistance to handling and chemical processes

During our process, we found that the nanostencil can be more resistant to dry handling processes and wet chemical processes. For example, for the evaporation process, we directly contacted the Ebeam patterned stencils on top of the target wafer. No gratings were damaged in this process. However, after washing our nanostencil in the Au etchant for a second use, most of the 1D gratings are damaged, even the thicker gratings ($w = 900 \text{ nm}$), were broken. The gratings tend to naturally attract each other in such processes. Critical drying could potentially mitigate this problem. Limited by the time given for this class, we did not explore on this topic.

At the same time, it turned out that 2D cross gratings fully survived the same chemical process. The geometry of the gratings prevents gratings from attracting each other from any direction. Therefore, we conclude that the 2D grating stencils are more reusable than the 1D ones.

3.2.2 Blurring due to shadowing and diffusion

Shadowing and diffusion both contribute to the blurring of final patterns on the substrate. They have different mechanisms, shown in Fig. 12. Shadowing effect assumes that evaporated metal particles travel in straight lines. A small gap would allow metal particles that travel at an oblique angle to pass through the nanoapertures and thus causing the broadening of the structures. The level of shadowing is fully determined by the relative geometry of the source, nanostencil and the target substrate during the evaporation. By contrast, diffusion assumes metal particles migrate in any direction. It happens not only during the evaporation, but also after the

evaporation at room temperatures. In addition, the extent of the diffusion strongly depends on the type of the metal and the substrate.

To study the effects of shadowing and diffusion, we compare the evaporated patterns under two evaporation conditions. The first one is the default setup on our AJA evaporator while the second one is a modified evaporation condition. The difference between these two conditions is shown in Table. 5. The details of the evaporation condition can be found in section 2.2.8.

Table. 5 Evaporation condition difference between first and second time.

	1st time	2nd time
Wafer rotation	Yes	No
Effective source size	5-7 mm	1 mm
Au deposition rate	2 A/s	0.5 A/s

Evaporation condition 1:

In Fig. 19, we show the SEM images of an evaporated pattern. We see that the Au nanorods that a flat and smooth top surface while the side walls are comprised of packed islands. The coalescence of dense Au particles during evaporation leads to the smooth surface. Processes such as diffusion and shadowing that has low density and energy lead to isolated grains. For this particular structure, the smooth top has about 790 nm width while the bottom is about 920 nm wide. It is expected that the total horizontal blurring caused by shadowing and diffusion is less than 100 nm on each side. However, it is difficult to determine the proportion between the two from our SEM images.

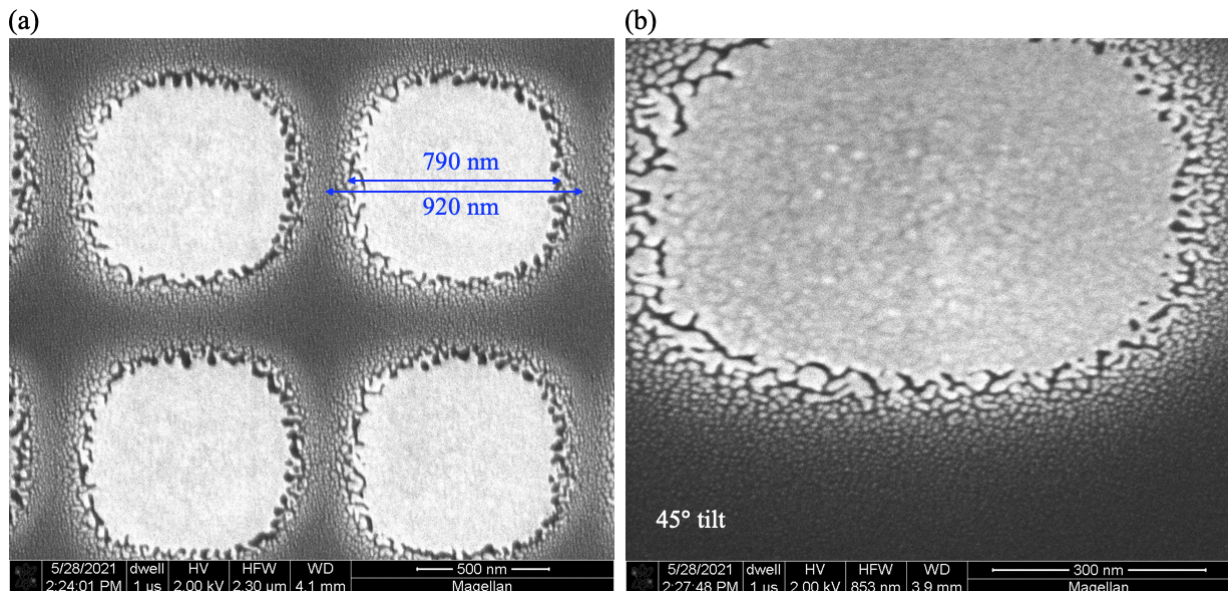


Fig. 19 SEM images of an evaporated pattern (under evaporation condition 1). a, 0° tilt. b, 45° tilt.

The SEM images of different patterns are shown in Fig. 20. The gratings seem to show similar extent of shadowing and diffusion as the square arrays shown in the previous figure. The Small

dot arrays (diameter less than 300 nm) show an increasing granular size towards the center without a smooth top. As we later confirmed with AFM images, the effective deposition rate through small apertures is much smaller than that of large apertures (see next section). This is expected to an intermediate state before a smooth top can be formed. As Fig. 20 (c) shows, the nano dots become in touch with each other when the period shrinks to 500 nm. With this evaporation condition, the resolvable periodicity is around 500 nm.

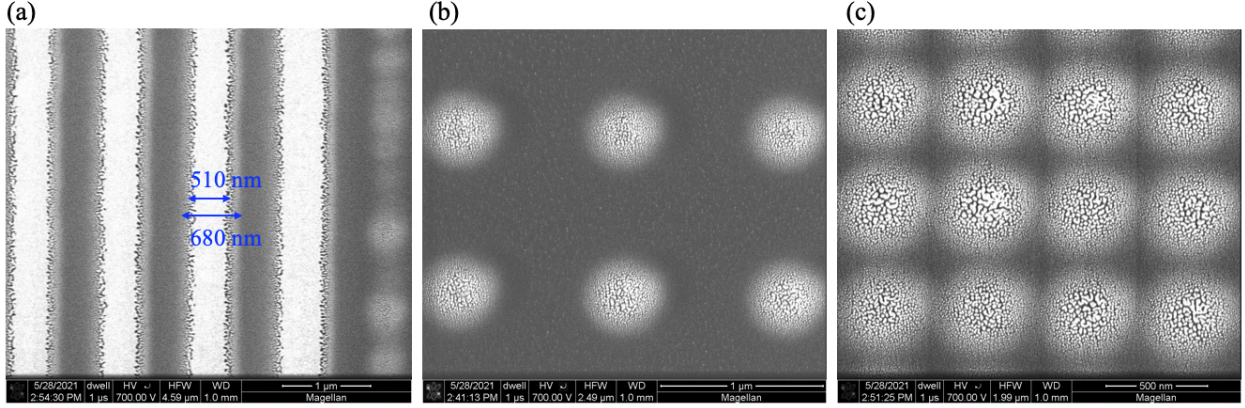


Fig. 20 SEM images of various geometries under evaporation condition 1. a, 1D gratings. b, Dot arrays ($p = 1 \mu\text{m}$). c, Dot arrays ($p = 500 \text{ nm}$)

Evaporation condition 2:

In Fig. 21, we show the SEM images of different patterns under evaporation condition 2. Note that these different patterns are scattered on a 4-inch wafer, the actual angle of the Au particles arriving on the pattern is different. A comet shaped pattern with a long tail appear in all geometries. The tails point towards different directions, indicating the shadowing happens at different angles. The longer the tail, the less contrast it has. This means the more spread out of the metal particles result in less thickness at each spot. At the same time, in directions without this tail, we don't observe much blurring of the structure. This indicates that the diffusion in these directions is negligible. The main contribution of the blurring comes from shadowing effect during the evaporation process.

In the square arrays, we can estimate the level of shadowing by drawing boxes. The solid box indicates the original shape of the aperture while the dotted lines outline the projected pattern. The square is smeared about 270 nm in the top middle case. Based on this, we come up with an equation that shows the relationship between smeared width Δw , evaporation angle θ and gap size d . The definition of these parameters is illustrated in Fig. 22.

$$\Delta w \approx d \sin \theta \approx d \frac{\Delta x}{l} \quad (1)$$

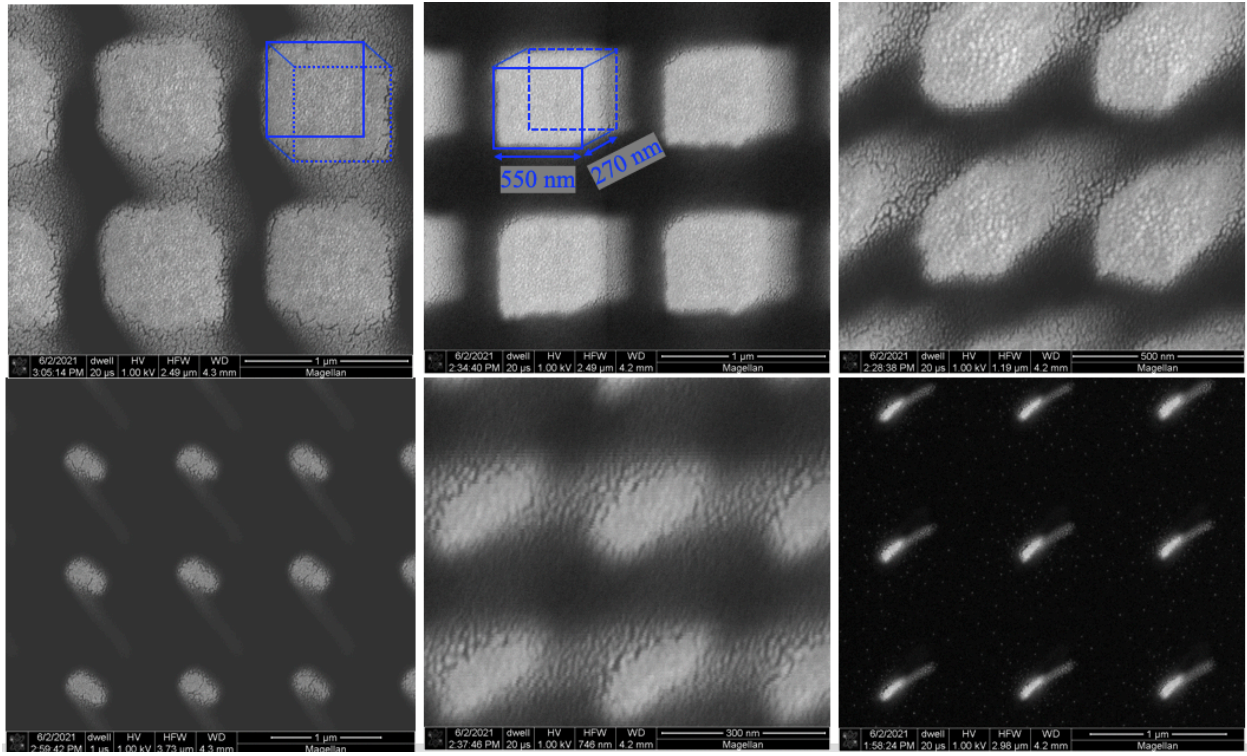


Fig. 21 SEM images of various geometries under evaporation condition 2. These different geometries experience different evaporation angles from the source and thus forming tails towards different directions.

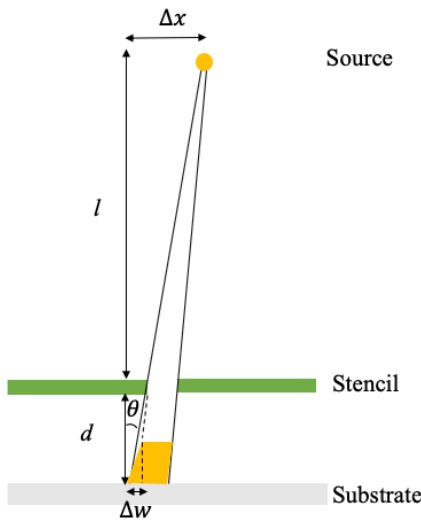


Fig. 22 Schematic of shadowing/smearing of the patterns at oblique angle.

This equation by no means gives an exact answer. But it reflects the relationship that the smeared width increases as the gap size and the evaporation angle get larger. From our best knowledge, $d \sim 5 \text{ um}$, $\Delta x \sim 3 \text{ cm}$, $l = 60 \text{ cm}$, giving rise to a smear width of $\Delta w \approx 250 \text{ nm}$. We expect this equation to give a result of the same order of magnitude as the exact answer. To sum up, the evaporation angle places a critical role in the shadowing effect. To reduce the shadowing effect, the evaporation angle should be as small and as collimated as possible.

Due to collimated angle arriving on the nanostencil, we start to see small features that are fully isolated from each other. As shown in Fig. 23, the features can be as small as $58 \text{ nm} \times 215 \text{ nm}$ with a periodicity of 300 nm . This shows that the resolution is better when the evaporation is more collimated.

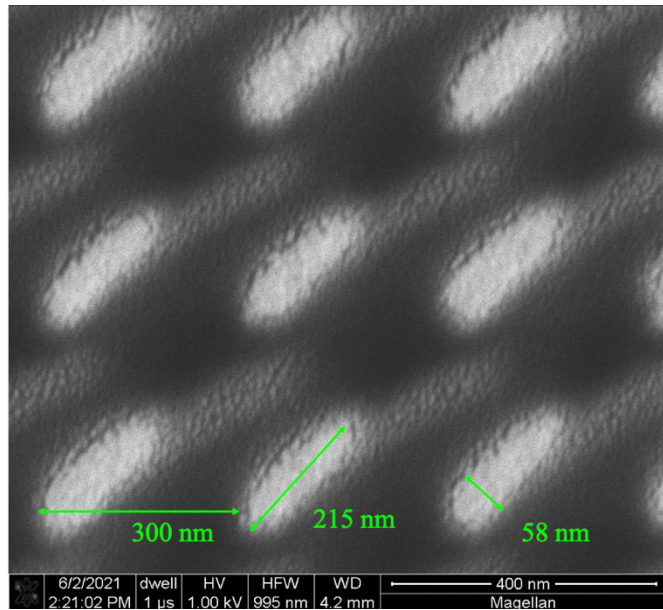


Fig. 23 SEM images of the smallest features resolved under evaporation condition 2.

Wafer bow measurement

We measured the bow size of different wafers to verify our estimated gap size. In Fig. 24, we show a data gained from our target wafer. The height variance from the edge to the center is about 2 um . Other wafers that are brand new or with LPCVD on both sides were also measured. The wafer bow size of all the 5 wafers we measured is less than 3 um . Therefore, we expect the gap size between two wafers resulting from the natural wafer bow should be less than 6 um . Depending on the clamping method, this gap size may vary.

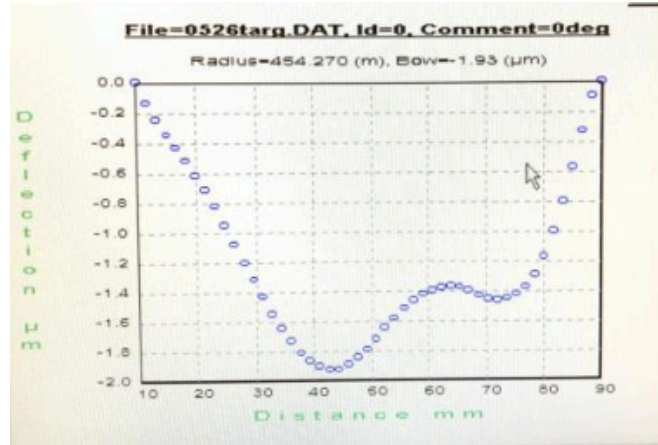


Fig. 24 Wafer bow measurement on target Si wafer.

3.2.3 Evaporation rate drops due to small apertures

By comparing AFM images of different patterns, we found that the effective deposition rate drops as the aperture size shrinks, shown in Fig. 25. The target evaporation thickness was 50 nm thick. Through apertures above 500 nm size, the height of the nanorods are the same as the target thickness. However, as the aperture decreases, the height of the nanorods decrease down to 15 nm. With the few data points, we fitted a curve of the projected evaporation rate through small apertures in Fig. 26. Please note that the actual rate depends also on the gap size, this only shows a relative rate when a few microns gap exists.

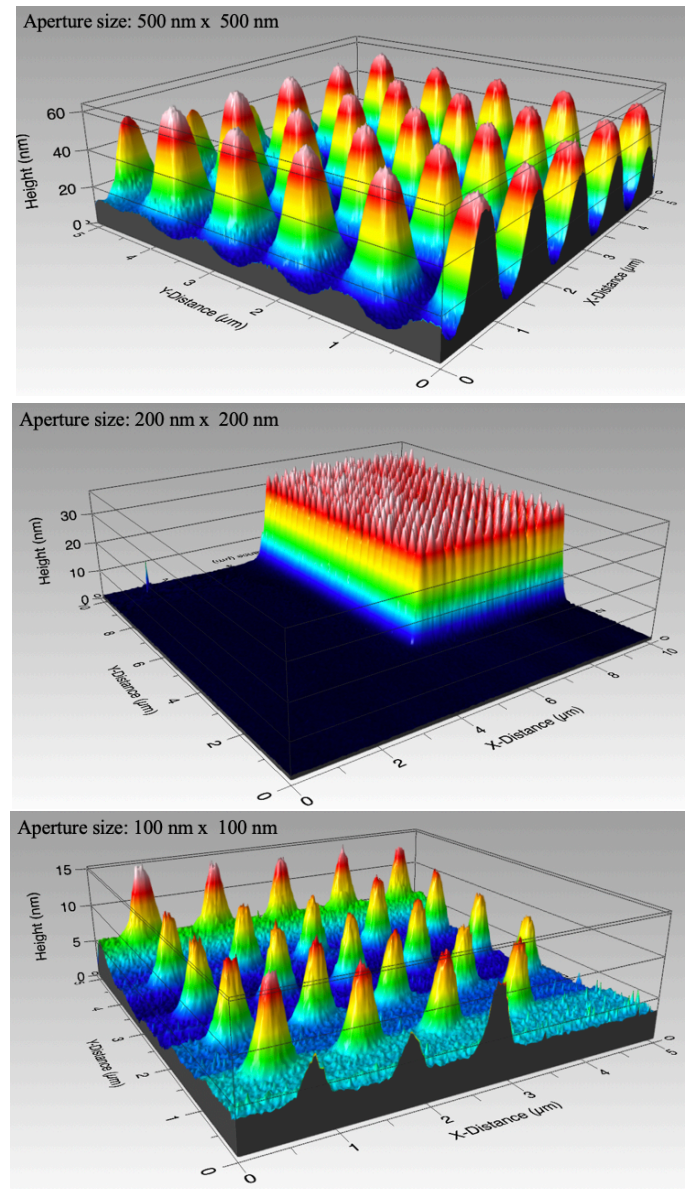


Fig. 25 AFM images of the evaporated metal patterns.

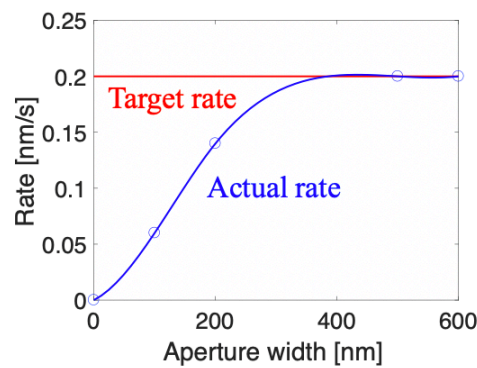


Fig. 26 Effective deposition rate through small apertures.

Conclusions

In our project, we explored on two topics. First, we studied how to enhance adhesion between Au and PDMS. Traditional method through metal adhesion layer (adhesion) causes cracks in the metal. A better way is to use self-assembled monolayer (MPTMS) to functionalize the surface. Second, we established a process flow of nanostencil lithography which can be applied to the patterning metal on a polymer substrate. We discovered that geometries strongly affect the mechanical stability of nanostencil. At the same time, the evaporated pattern on the substrate can be blurred due to shadowing and diffusion effect. The shadowing effect, being the dominant factor, can be significantly reduced by controlling the evaporation angle and source size. The smallest resolved features using nanostencil lithography is around 60 nm.

Future Work

We plan to explore 2 future directions to complement this work. We want to start with more methods to reduce shadowing effect. We plan to further control the evaporation direction and minimize the gap size. Afterwards, we want to test this method with different combination of metal and polymer substrate.

Acknowledgement

The authors want to thank the instructors and the mentors who contributed a lot of the creative ideas and helpful suggestions. In addition, we want to thank Rich Tiberio for his technical advices on e-beam lithography and metal evaporation process. We want to thank Maryann Tung for the help in high quality SEM images. We want to acknowledge Usha Raghuram, Maurice Stevens, Michelle Rincon, and Marcin Markiewicz on technical discussions on specific tools. We want to show our appreciation to Ludwig Galambos on various advice on a broad range of tools.

Part of this work was performed at Stanford Nano Facilities (SNF). Part of this work was performed at the Stanford Nano Shared Facilities (SNSF), supported by the National Science Foundation under award ECCS-1542152.

The project is funded by class E241 and Intermolecular Inc.

Budget

In this class, we used over 30 kinds of tools to accomplish our project. Here we list the contribution from a few specific tools.

Item	Expense
Training	\$691
Wafers and supplies	\$560
AJA	\$273
Metals	\$404.36
Ebeam	\$589.58
Heidelberg	\$67.67
Others (wet benches, SEM, AFM, etc.)	\$2247.39
Total	\$4833

References

1. Atmaja, B., Frommer, J. & Scott, J. C. Atomically Flat Gold on Elastomeric Substrate. *Langmuir* **22**, 4734–4740 (2006).
2. Sinha, A., Lee, J., Li, S. & Barbastathis, G. Lensless computational imaging through deep learning. *Optica* **4**, 1117–1125 (2017).
3. Byun, I., Coleman, A. W. & Kim, B. Transfer of thin Au films to polydimethylsiloxane (PDMS) with reliable bonding using (3-mercaptopropyl)trimethoxysilane (MPTMS) as a molecular adhesive. *J. Micromechanics Microengineering* **23**, 85016 (2013).
4. Vazquez-Mena, O., Gross, L., Xie, S., Villanueva, L. G. & Brugger, J. Resistless nanofabrication by stencil lithography: A review. *Microelectron. Eng.* **132**, 236–254 (2015).
5. Pang, S. W. *et al.* Pattern transfer by dry etching through stencil masks. *J. Vac. Sci. Technol. B Microelectron. Process. Phenom.* **6**, 249–252 (1988).
6. Sidler, K. *et al.* Organic thin film transistors on flexible polyimide substrates fabricated by full-wafer stencil lithography. *Sensors Actuators A Phys.* **162**, 155–159 (2010).
7. Bao, W. *et al.* In situ observation of electrostatic and thermal manipulation of suspended graphene membranes. *Nano Lett.* **12**, 5470–5474 (2012).
8. Allenspach, R., Bischof, A., Stampanoni, M., Kerkemann, D. & Pescia, D. Growing thin magnetic films with a mask: Distinguishing between magnetic and instrumental asymmetries. *Appl. Phys. Lett.* **60**, 1908–1910 (1992).
9. Salis, G., Fuhrer, A., Schlittler, R. R., Gross, L. & Alvarado, S. F. Temperature dependence of the nonlocal voltage in an Fe/GaAs electrical spin-injection device. *Phys. Rev. B* **81**, 205323 (2010).
10. Vazquez-Mena, O. *et al.* Analysis of the blurring in stencil lithography. *Nanotechnology* **20**, 415303 (2009).

11. Cojocaru, C.-V. *et al.* Complex oxide nanostructures by pulsed laser deposition through nanostencils. *Appl. Phys. Lett.* **86**, 183107 (2005).
12. Vazquez-Mena, O. *et al.* High-Resolution Resistless Nanopatterning on Polymer and Flexible Substrates for Plasmonic Biosensing Using Stencil Masks. *ACS Nano* **6**, 5474–5481 (2012).
13. Engineering, C. Nonlocal Metasurfaces for Optical Signal Processing. *Phys. Rev. Lett.* **121**, 173004 (2018).